On-orbit beam pointing calibration for nanosatellite laser communications

Ondrej Čierny
Kerri L. Cahoy

On-orbit beam pointing calibration for nanosatellite laser communications

Ondrej Čierny[*] and **Kerri L. Cahoy**
Massachusetts Institute of Technology, Space Telecommunications, Astronomy, and Radiation Laboratory, Department of Aeronautics and Astronautics, Cambridge, Massachusetts, United States

Abstract. We describe techniques developed to optimize beam pointing control for a CubeSat laser downlink demonstration mission being developed at the MIT Space Telecommunications, Astronomy, and Radiation Laboratory. To fine-point its downlink beam, the mission utilizes an uplink beacon signal at 976 nm captured by an on-board ± 5- deg field-of-view detector and tracked by a 3.6-mm commercial, off-the-shelf MEMS fast steering mirror. As these miniature actuators lack feedback sensors, the system design is augmented with an optical calibration signal to provide the mirror's pointing feedback. We describe the system and introduce calibration algorithms utilizing the feedback signal to achieve higher fidelity beam pointing control. A demonstration in the laboratory is conducted to obtain a quantitative performance analysis using quasi-flight hardware with simulated spacecraft body pointing disturbances. Experimental results show that beacon tracking errors of only 16 μrad root-mean-square are feasible for both axes, significantly exceeding the mission pointing requirement of 0.65 mrad and indicating the feasibility of narrower beams and higher data throughputs for next-generation downlink demonstration missions. © *The Authors. Published by SPIE under a Creative Commons Attribution 3.0 Unported License. Distribution or reproduction of this work in whole or in part requires full attribution of the original publication, including its DOI.* [DOI: 10.1117/1.OE.58.4.041605]

Keywords: laser communications; calibration; pointing; tracking.

Paper 181420SS received Oct. 1, 2018; accepted for publication Oct. 26, 2018; published online Nov. 21, 2018.

1 Introduction

As more complex and data-intensive instruments get incorporated into nanosatellite mission designs, such as multiband radiometers[1] or hyperspectral imagers,[2] the downlink demand of these satellites can rapidly grow up to a point where it becomes impractical to use traditional radio-frequency communications. Laser communication (lasercom) is a contender to overcome this bottleneck and provide higher throughput communications while reducing the necessary volume, weight, and power requirements on the satellite platforms. Because nanosatellite resources are highly constrained, these benefits can allow for new mission concepts.

To demonstrate the feasibility of lasercom downlinks from a nanosatellite platform, the MIT Space Telecommunications, Astronomy, and Radiation (STAR) Lab is developing a low-cost CubeSat optical communications terminal,[3] which is currently being integrated. The terminal is 1.2U in volume and weighs roughly 800 g. For communications, it leverages commercial, off-the-shelf (COTS) optical components, such as an erbium-doped fiber amplifier and a laser transmitter at 1550 nm. The output beam has an average power of 200 mW and is modulated using pulse position modulation. This approach has benefits in both power efficiency and thermal management[4] (both of which are challenges on CubeSats) and allows for 10 to 40 Mbps downlink rates depending on the receiver aperture.

One of the primary challenges that arise when developing a miniature-scale lasercom terminal, especially in a bus-agnostic configuration, is to achieve sufficiently accurate downlink beam pointing. For this reason, the MIT terminal is to demonstrate its own fine pointing system (FPS) that will be able to reject up to ± 5 deg of bus-introduced attitude control error during a ground track maneuver. The designed FPS utilizes a reference optical beacon signal from the ground station that is tracked on-orbit using a miniature MEMS fast steering mirror (FSM). Using this technique, alignment between the optical receiver and transmitter can be established even in presence of significant platform pointing errors.

During the past 2 years, there has been significant progress in achieving highly accurate pointing control on CubeSats. The most notable missions include the Arcsecond Space Telescope Enabling Research in Astrophysics (ASTERIA), a 6U CubeSat built by the NASA Jet Propulsion Laboratory; the Miniature X-ray Solar Spectrometer (MinXSS), a 3U CubeSat designed by the University of Colorado Boulder; and the Optical Communications and Sensor Demonstration (OCSD), a 1.5U CubeSat built by the Aerospace Corporation. ASTERIA has shown particularly impressive results in star tracking stability. Using a highly precise commercial bus attitude determination and control system (ADCS) and a custom piezo-steered focal plane array, a stability of 2.4 μrad was achieved over 20 min.[5] MinXSS used the same bus ADCS as ASTERIA without a fine pointing stage on its payload and achieved <58 μrad pointing precision[6] while analyzing soft solar x-ray spectra.

While these two missions demonstrate superior pointing stability in tracking very distant objects, performance in ground tracking or beam steering was not reported. For low Earth orbit (LEO) ground station tracking, it is a greater challenge to maintain precision pointing while slewing the spacecraft. In a typical 400-km LEO, the satellite must slew itself up to around 1 deg/s. This places much more stress on the ADCS as opposed to when the spacecraft is staring at a distant celestial object.

*Address all correspondence to: Ondrej Cierny, E-mail: ondrej@mit.edu

OCSD, being mainly an optical downlink demonstrator, is a more analogous mission to the MIT downlink terminal since it requires precise ground tracking. OCSD uses a custom-developed body ADCS to point its downlink beam and achieved a 350-μrad pointing accuracy.[7] However, none of the mentioned missions utilized a ground-based beacon or an FSM for platform disturbance rejection. Precise beam pointing control has not yet been demonstrated using these technologies on nanosatellites.

One problem in using off-the-shelf MEMS FSMs for pointing control is that they usually lack feedback sensors. Generally, the FPS has to rely on the device's open-loop voltage-to-angle transfer functions. However, Riesing[8] showed that different thermal modes can affect the device characteristics, leading to errors of up to 0.15 mrad. Additional effects studied included hysteresis, repeatability, and nonlinearity, and in the worst case, added up to an additional 80 μrad of error. These errors were studied on FSMs with a smaller mechanical steering range of ± 1 deg. The current terminal design is based on ± 3 deg FSMs, which decreases the control resolution (the same driving electronics are utilized), and so, the open-loop errors are expected to be higher.

Another major issue is optomechanical misalignment between the beacon detector and the FSM optical axes, which is susceptible to thermal deformation and vibration. If this deviation is not exactly known, it directly translates to pointing error with regards to the receiver. Although these errors are not critical in terms of the current mission objectives, they motivated research[9] in developing a calibration procedure for the FSM based on a custom optical FSM feedback signal.

In this work, we focus on beam pointing calibration using an optical FSM feedback signal that is added to the FPS system design. We present an architecture that multiplexes a calibration laser with the transmission laser and samples the FSM pointing angle on the same detector that is used for beacon tracking. This approach reduces the complexity and the number of needed parts in the optical design.

We introduce algorithms developed to utilize the feedback signal for calibration and higher fidelity beam pointing control. The calibration allows for precise beacon tracking regardless of misalignment between the detector and the FSM or variations in the FSM characteristics. The implemented algorithm is capable of quick calibration and can be executed before each ground station overpass. To validate the approach and obtain a quantitative pointing performance assessment, we built a laboratory testbed with quasi-flight FPS hardware and a setup to simulate spacecraft pointing disturbances. We present the experiment and the metrics obtained from an end-to-end pointing accuracy analysis using two different control approaches.

The paper is structured into four major sections. Section 2 introduces the overall design of the FPS. Section 3 is focused on beam pointing control with the calibration signal added to the system. Section 4 describes how the on-orbit calibration algorithm is implemented. Finally, Sec. 5 covers the laboratory testbed, the test scenario, and analysis of the experimental results.

2 Fine Pointing System Concept

From an operational standpoint, the optical downlink is established over three major overlapping phases. In the first phase, the spacecraft initiates a slew maneuver to coarsely point the optical terminal at the optical ground station (OGS). This step ensures that the beacon will be visible within the beacon detector's field-of-view. In the second phase, the OGS will begin to track the satellite as it passes over and transmits the beacon to facilitate the fine pointing of the downlink beam. During the final phase, the beacon is acquired on the detector and the FPS begins tracking the signal with the FSM, making the system ready for data transmission.

To close the link with conservative margin for an initial demonstration, link budget analysis[3] set the downlink beam divergence to 1.3 mrad full-width at half-maximum (FWHM). For pointing loss, 3 dB is budgeted, which means the FPS has to keep the beam pointed within the FWHM from the OGS. This sets the absolute pointing accuracy requirement to ± 0.65 mrad.

2.1 Optomechanical Design

The key aspect of the FPS is that the beacon detector provides a reference to be tracked by the FSM, which steers the transmission signal. The beacon detector itself consists of a focal plane array (FPA) and a focusing lens assembly (LA). To augment this system with a calibration capability, we multiplex the 1550-nm transmission signal with a 635-nm calibration signal in a wavelength division multiplexer (WDM). A dichroic beamsplitter (DBS) is then added in front of the beacon detector so that the steered multiplexed beam is "decoupled" in free space. This way, the transmission signal is reflected toward the OGS while the calibration signal can be seen on the beacon detector. The DBS is COTS from Thorlabs and has a roughly 99% reflectance at 1550 nm and 6% at 976 and 635 nm. A depiction of this architecture is shown in Fig. 1. Note that we ignore the DBS reflections, which are not relevant to the FPS. The small fraction of the transmitted 1550 nm signal is not seen on the FPA as it is a silicon-based detector. The 976-nm reflection is also not relevant and is severely attenuated in case it reaches the FPA again due to specular reflections. The same holds true for the other optical paths of the 635-nm signal. The side
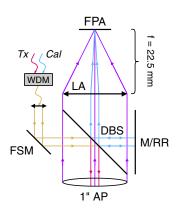

Fig. 1 Optical diagram of the FPS. The transmit (Tx, red) and calibration (Cal, blue) signals are multiplexed in a WDM and then split on a DBS to provide a feedback of the FSM pointing angle. A mirror/retroreflector (M/RR) is used to reflect the calibration signal onto the FPA. The Tx signal leaves the system through the main 1" aperture (AP), which also serves for beacon reception (purple). Note that signal reflections that are not relevant to the FPS are not displayed in this diagram.

mirror ensures reflection of a small portion of the calibration signal back toward the beacon detector. It is, however, currently being replaced in the design with a retroreflector so that there can be no bias in the feedback signal due to imperfect mirror alignment, which would be challenging to correct on-orbit.

Apart from the structure, all the FPS-related optomechanical components are COTS, making the system a very low-cost solution. The FPA is based on a camera with a monochromatic CMOS Aptina MT9P031 sensor that has prior space heritage.[10,11] This 1/2.5" array has a small pixel pitch of 2.2 μm and a quantum efficiency of roughly 4% at 976 nm, which is sufficient for beacon detection.[12] The LA is from Schneider Optics Xenoplan series, with an effective focal length of 22.5 mm. The combination yields a vertical field-of-view (FoV) of roughly 5.4 deg (half angle) and horizontal FoV of 7.2 deg. The MEMS FSM is from Mirrorcle Technologies with a mirror diameter of 3.6 mm and mechanical steering range of ±3 deg, which enables optical scanning of ±6 deg. Overall, the system enables bus pointing error rejection limited by the minimum beacon FoV of 5.4 deg.

The other optical components are all off-the-shelf parts from Thorlabs. The collimator is tuned for 1550 nm, so some defocus is present on the calibration spot due to chromatic aberration, but it does not pose a major problem with regards to centroiding. For manual control of the calibration laser power, a variable optical attenuator is also added between the WDM and the calibration laser diode.

3 Pointing Control

To align the ground receiver with the optical transmitter, the control objective is to track the incident beacon off-boresight angle with the transmit beam off-boresight angle. In an ideal system, the beacon incidence angle is given through the FPA measurements as follows:

$$\tan \theta_{B,X/Y} = \frac{\mu \, p_{B,X/Y}}{f}, \qquad (1)$$

where f is the effective focal length of the LA, μ is the pixel pitch, and $p_{B,X/Y}$ is the centroid of the beacon spot on the FPA relative to its center. If conventional open-loop pointing is utilized, the FSM has to be mechanically steered to reach the same optical deflection of the transmit beam given by

$$\theta_{\mathrm{FSM},X/Y} = \frac{1}{2} \arctan \frac{\mu p_{B,X/Y}}{f}. \qquad (2)$$

The required FSM angles would then have to be transformed into control inputs via a predefined transfer function, look-up table or similar. There are several sources of error with this approach:

1. Any misalignment of the FSM with regards to the FPA results in a pointing bias.
2. Imperfections in the FPA/LA system give errors in the calculation of $\theta_{B,X/Y}$.
3. The FSM response varies as a function of temperature.

Compensating for these errors would be possible to a certain extent, but not trivial. To reduce pointing bias, the OGS would have to uplink the received power levels at ground and
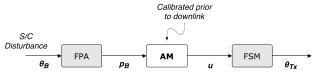

Fig. 2 Diagram of calibrated open-loop pointing.

the transmitter would need to search for a maximum. This is particularly challenging due to varying link distance and fading of the signal in the atmosphere. To correct for the FSM response changes, software compensation could be implemented if temperature sensing is implemented and the device is rigorously characterized under different temperatures.

The calibration laser simplifies the tracking approach as it enables mapping the FSM angle relative to the reference frame of the beacon measurements. This way the mentioned error sources are avoided without any complex countermeasures. The control objective is reduced to tracking the centroid of the beacon with the centroid of the calibration laser on the FPA.

To approximate the FSM input signal to the centroid measurements in a robust way, we introduce a simple affine map (AM) given by

$$\begin{bmatrix} u_X \\ u_Y \end{bmatrix} = \begin{bmatrix} a_{xx} & a_{xy} \\ a_{yx} & a_{yy} \end{bmatrix} \begin{bmatrix} p_{C,X} \\ p_{C,Y} \end{bmatrix} + \begin{bmatrix} t_x \\ t_y \end{bmatrix}, \qquad (3)$$

where $u_{X/Y}$ are the FSM control inputs and $p_{C,X/Y}$ are the centroid values of the calibration laser within the FPA. If the parameters of the AM are calibrated on-orbit, it is possible to drive the FSM in two modes: in calibrated open-loop pointing (without real-time utilization of the feedback signal) or in closed-loop pointing (feedback signal is actively sampled during beam control).

3.1 Calibrated Open-Loop Pointing

This regime is depicted in Fig. 2. The FPA is used solely as a beacon detector during a downlink and the AM is calibrated before the link is initiated. As the AM is a linear transformation, this approach still suffers from FSM nonlinearities and repeatability error. However, it solves problems related to optomechanical misalignment and shifts in the FSM response. Implementation wise, this approach requires less complexity, as the calibration laser is switched off and cannot interfere with the beacon readings.

3.2 Closed-Loop Pointing

This architecture is shown in Fig. 3. To achieve closed-loop control, the FPA must continuously sample both the beacon and the calibration laser centroids. This requires a careful sampling technique so that the signals can be extracted
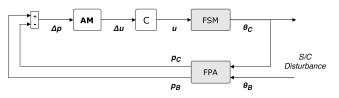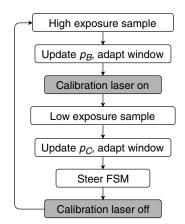

Fig. 3 Diagram of closed-loop pointing.

Fig. 4 Sampling technique utilized during closed-loop pointing.

without mutual interference. The benefit is that this scheme can further reject tracking errors caused by nonlinearities or repeatability, as we can make the angles converge using a controller (C).

We implement two steps to minimize the sampling interference. First, we exploit the dynamic range of the FPA as much as possible. Since the beacon signal is of very low power due to free-space path loss, it requires high exposure times on the FPA. On the contrary, we fine-tune the calibration laser power internally so that it can be sampled with the lowest exposure time on the FPA. As this difference is several orders of magnitude, it minimizes the effect of the beacon when sampling the FSM feedback. Second, to prevent the FPA from being blinded when the beacon is sampled, the calibration laser is switched off in-between beacon measurements. Overall, this results in a sample switching sequence, where low and high exposure frames are captured in an alternating manner. This technique is depicted in Fig. 4.

To maximize the sampling rate, the FPA is operated in a windowed mode so that only a small region of interest around the centroid is read out. Once the signals are sampled, the tracking error is transformed to FSM-space with the AM and fed into a controller that drives the FSM.

4 Calibration Algorithm

Estimating the AM precisely is critical for optimal performance of the FPS. Given the fact that it is very sensitive to the system alignment and the device response, it is desirable to have the option to re-estimate it quickly at any point. For high robustness and accuracy, we propose a calibration algorithm consisting of an automated sample collection and estimation of the AM as a least-squares error minimization problem.

4.1 Sample Collection

A quick automated measurement is performed to obtain the samples needed for estimation of the AM. The FSM is given gradually changing control inputs and the resulting centroids of the feedback signal are collected from the FPA. We steer the FSM in a spiral pattern during the measurement as it gives two advantages: (1) the spiral is easy to implement in a parameterized fashion so that the desired number of samples and their density can be tweaked easily using the frequency of sines and cosines and (2) the density decreases outward from the center, which follows the assumption

that statistically the pointing error is expected to be distributed around zero.

In the initial step, N FSM control inputs are generated, where N is our calibration input parameter that in a sense specifies how fast versus how accurate the estimation should be.

Let:

$$n = [0, 1, 2, \ldots, N-1], \tag{4}$$

$$a_i = \frac{u_{\max}}{N-1} n_i, \tag{5}$$

$$\omega = \pi \frac{\sqrt{N}}{N}, \tag{6}$$

where n_i are point indices, a_i are growing spiral amplitudes scaled to the maximum FSM input $u_{\max}$, and ω is angular frequency distributing points within the spiral. We define the FSM control inputs as follows:

$$u_{X,i} = a_i \cos \omega n_i, \tag{7}$$

$$u_{Y,i} = a_i \sin \omega n_i. \tag{8}$$

The FSM is then gradually steered toward each u_i and the resulting $p_{C,i}$ are collected for estimation of the AM.

4.2 Affine Map Estimation

Having a set of control inputs u_i and corresponding centroid measurements $p_{C,i}$, it is helpful to establish the following notations:

$$\bar{x} = \frac{1}{N} \sum_{i=1}^{N} x_i, \tag{9}$$

$$\tilde{x}_i = x_i - \bar{x}, \tag{10}$$

where $\bar{x}$ is the center of mass of a set of points, and $\tilde{x}_i$ denotes the centered points. Recalling the AM definition in Eq. (3), we know that to derive an optimal AM from the set of samples in a least-squares fashion, minimization of the following error criterion is sought:

$$f(A, t) = \sum_{i=1}^{N} \|A p_{C,i} + t - u_i\|^2. \tag{11}$$

The objective is to find a solution over all possible matrices A and vectors t such that the gradient of f vanishes. It can be shown with an intrinsic proof[13] that if $N > 3$ and the samples are not constrained within a subdimension (e.g., a line), the criterion is convex and has exactly one minimum defined as follows:

$$A = \left(\sum_{i=1}^{N} \tilde{u}_i \tilde{p}_{C,i}^t \right) \left(\sum_{i=1}^{N} \tilde{p}_{C,i} \tilde{p}_{C,i}^t \right)^{-1}, \tag{12}$$
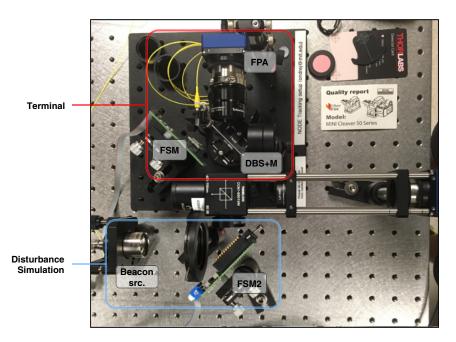
$$t = \bar{u} - A \bar{p}_C. \tag{13}$$

Fig. 5 The optical testing bench setup in the laboratory.

5 Experiment

To test the developed calibration and beam control techniques, a laboratory testbed is assembled based on the system design and the selected hardware. The primary optical components are mounted on an optical breadboard. This includes the FPA, LA, and DBS with a side mirror, FSM, and collimator. The optics are manually spaced such that they are as close as possible to the mechanical structure designed for the CubeSat terminal. The calibration optical path is established by connecting a 635-nm fiber coupled laser to the collimator through the WDM. The second WDM channel is left unconnected as the transmission laser is not needed for beam pointing experiments.

In order to simulate the spacecraft body pointing disturbances, we add additional optics to create a beacon signal on the test bench. Since a body pointing error is effectively seen on-orbit as drift of the beacon signal across the FPA, we can accomplish the same result using an extra FSM that steers the incident beacon signal. The overall optical setup can be seen in Fig. 5.

The calibration and control algorithms are implemented on the selected payload microcontroller (PMC), which is based on a Raspberry Pi Compute Module. The PMC interfaces to the FPA using a standard USB link and to the FSMs through drivers provided by Mirrorcle Technologies. The drivers contain digital-to-analog converters commanded via a serial peripheral interface bus and a low-pass filter to facilitate driving of the FSMs. The calibration laser source is controlled through the PMC as well as via a general purpose input-output (GPIO) connection that switches the laser on and off. For the purposes of the experiment, the PMC also controls the beacon disturbance setup and acts as a data acquisition unit. The whole experiment is monitored and controlled via an external laptop, which connects to the PMC via a universal asynchronous receiver–transmitter interface utilizing the point-to-point protocol. The complete experiment architecture is visualized in Fig. 6.

5.1 Test Scenario

To obtain a quantitative measure of the FPS performance with calibration, an experiment is designed so that the FPS is exercised similarly to what is expected during a ground station overpass. The test scenario is based on a 400-km altitude LEO, with an overpass duration of roughly 10 min. A 10-s calibration is performed prior to the overpass, which corresponds to estimation of the AM using 100 samples from the FPA. For disturbance simulation, data obtained from a potential spacecraft bus provider are used to generate an error distribution that is injected into the system through the external beacon-steering FSM. A summary of the orbit configuration and disturbance parameters is given in Table 1.

We conduct tests for both the calibrated open-loop pointing and the closed-loop pointing modes. In the first case for open-loop, the calibration laser is not utilized to drive the FSM (architecture follows Fig. 2), but we still sample and store it for analyzing the beacon tracking performance. In the second case for closed-loop, we feed the control error directly into an integral controller that drives the FSM. The controller response is tuned in a simulation by modeling the FSM and sampling dynamics. In both cases, the FSM is driven at about 30 Hz, limited by the FPA sampling rate. For performance assessment, the centroid tracking errors are stored for the duration of the whole test and angular pointing errors are derived using Eq. (1).

5.2 Results

Figures 7 and 8 show the recorded open-loop pointing error as an aperture-plane scatter plot and in a histogram form. The circle corresponds to the derived ±0.65 mrad pointing accuracy requirement given the mission link budget. To obtain performance metrics, we fit the data with probability distribution functions and calculate the pointing error mean and standard deviation. The orthogonal components are fit to a Gaussian and the error magnitude to a Rician distribution.

Fig. 6 Diagram of the whole experimental setup.

Table 1 Test scenario assumptions.

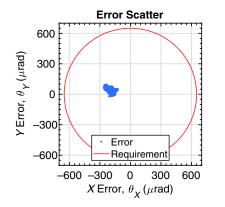| Parameter	Value	Notes
Orbit	400 km	Standard LEO
Overpass time	10 min	Horizon-to-horizon
Calibration	100 samples	No estimation improvement found for more samples[9]
ADCS bias	1 deg	S/C bus-to-payload misalignment
ADCS accuracy	0.15 deg (3σ)	S/C bus vendor performance metrics
ADCS stability	0.0225 deg/s (3σ)	S/C bus vendor performance metrics
ADCS jitter	N/A	Not characterized by vendor/impractical to inject

Fig. 7 Scatter plot of the tracking error obtained during the open-loop pointing test. The ±0.65 mrad pointing requirement is visualized as a red circle.

Fig. 8 Statistical analysis of the error distribution in the open-loop test. The orthogonal component histograms are fit to a Gaussian and the magnitude histogram is fit to a Rician distribution.

The metrics are summarized below in Table 2. We can observe that in this regime, a pointing bias is present, which is mainly attributed to linear approximation of the system and FSM repeatability, and is in line with Riesing's[8]
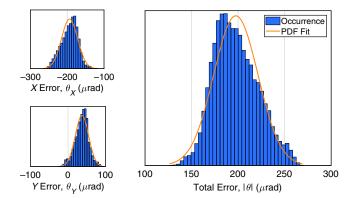
findings. However, the FPS is still well within the mission requirement of ±0.65 mrad with significant margin.

In Figs. 9 and 10, results of the closed-loop pointing test are shown. The closed-loop mode shows significant tracking

Table 2 Tracking performance metrics obtained through statistical analysis.

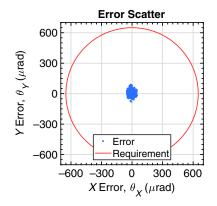|	Open-loop		Closed-loop	
	Mean (μrad)	σ (μrad)	Mean (μrad)	σ (μrad)
θ_X	−193.5	22.0	0.09	15.6
θ_y	36.9	17.7	−0.31	16.4
$|\theta|$	197.5	23.8	20.0	10.5
$|\theta_{REQ}|$	650 μrad			

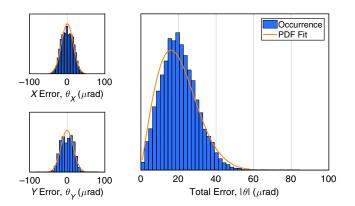**Fig. 9** Scatter plot of tracking error obtained during the closed-loop pointing test.

Fig. 10 Statistical analysis of the error distribution in the closed-loop test. The orthogonal component histograms are fit to a Gaussian and the magnitude histogram is fit to a Rayleigh distribution (reduced Rician distribution as the mean of the orthogonal components is zero).

accuracy improvements, mainly due to rejection of steady-state errors. The error is distributed around zero for both orthogonal components, with a standard deviation of roughly 16 μrad. The total error magnitude has a mean of 20 μrad and standard deviation of 10.5 μrad. This is a significant improvement from the open-loop case, which resulted in a mean error of roughly 200 μrad and a standard deviation of 24 μrad.

We trace the remaining error to two primary sources: (1) lag between calibration and beacon signal samples, which significantly limits the controller bandwidth, and

(2) background noise on the FPA, which leads to noise in signal centroiding.

Given these findings, if a closed-loop pointing error of roughly 50 μrad (3σ) is reached during operation, it would result in essentially negligible pointing loss (−0.005 dB) with the current downlink beam divergence. This is good motivation to pursue narrower beams and aim for higher downlink rates in next-generation demonstration missions.

A few hardware and software upgrades should be considered for further tracking accuracy improvement. A higher degree of freedom nonlinear mapping (e.g., based on radial basis functions[13]) between the FSM inputs and centroid outputs could result in improved open-loop pointing, especially at higher off-boresight angles. With regards to closed-loop pointing, a higher frame rate FPA that allows driving the FSM at faster rates than 30 Hz could be investigated. This would reduce the sample delays while also possibly enabling sample averaging for reduced centroiding noise.

6 Conclusion

This paper presents calibration techniques that were developed to optimize beam pointing on a low-cost nanosatellite laser downlink demonstration terminal. Rather than relying on the open-loop response characteristics of the beam-steering MEMS FSM, we introduce an architecture that provides optical feedback of the FSM pointing angle relative to the beacon incidence angle. This design enables rejection of errors due to system misalignment or due to shifts in the FSM characteristics. We introduce an approach that facilitates simultaneous sampling of the beacon and the calibration signal on a single detector. A robust calibration algorithm that estimates a map between the FSM control inputs and detector readings is presented. The designed technique allows for two distinct operation modes: a calibrated open-loop tracking mode and a closed-loop tracking mode.

Experimental results obtained from an end-to-end test scenario in the laboratory show that both operational modes significantly exceed the mission required tracking accuracy of ±0.65 mrad. In the calibrated open-loop mode, the total tracking error had a mean of 200 μrad and a standard deviation of 24 μrad. In the closed-loop mode, the total tracking error is significantly reduced with a mean of 20 μrad and a standard deviation of 10.5 μrad. This corresponds to almost negligible pointing loss in the current mission design and motivates for higher performance next-generation nanosatellite lasercom demonstrations.

References

1. S. R. Tsitas and J. Kingston, "6U CubeSat design for earth observation with 6-5m GSD, five spectral bands and 14Mbps downlink," *Aeronaut. J.* **114**, 689–697 (2010).
2. D. Mandl et al., "Hyperspectral Cubesat constellation for natural hazard response (follow-on)," in *Proc. of the 30th Annual AIAA/USU Conf. on Small Satellites*, SSC16-XII-02 (2016).
3. E. Clements et al., "Nanosatellite optical downlink experiment: design, simulation, and prototyping," *Opt. Eng.* **55**, 111610 (2016).
4. E. Clements et al., "Integration and testing of the nanosatellite optical downlink experiment," in *Proc. of the 32nd Annual AIAA/USU Conf. on Small Satellites*, SSC18-XII-05 (2017).

5. C. M. Pong, "On-orbit performance and operation of the attitude and pointing control subsystems on ASTERIA," in *Proc. of the 32nd Annual AIAA/USU Conf. on Small Satellites*, SSC18-PI-34 (2018).
6. J. Mason et al., "MinXSS-1 CubeSat on-orbit pointing and power performance: the first flight of the blue canyon technologies XACT 3-axis attitude determination and control system," *JoSS* **6**(3), 651–662 (2017).
7. T. Rose et al., "Optical communications downlink from a 1.5U CubeSat: OCSD program," in *Proc. of the 32nd Annual AIAA/USU Conf. on Small Satellites*, SSC18-XI-10 (2018).
8. K. M. Riesing, "Development of a pointing, acquisition, and tracking system for a nanosatellite laser communications module," Master's Thesis, Massachusetts Institute of Technology (2015).
9. O. Cierny, "Precision closed-loop laser pointing system for the nanosatellite optical downlink experiment," Master's Thesis, Lulea University of Technology and Julius Maximilians University of Wurzburg (2017).
10. J. Enright, D. Sinclair, and K. C. Fernando, "COTS detectors for nanosatellite star trackers: a case study," in *Proc. of the 25th Annual AIAA/USU Conf. on Small Satellites*, SSC11-X-1 (2011).
11. L. McNutt et al., "Near-earth asteroid scout," in *AIAA Space Conf.*, San Diego, California (2014).
12. T. Nguyen, "Laser beacon tracking for free-space optical communication on small-satellite platforms in low-earth orbit," Master's Thesis, Massachusetts Institute of Technology (2015).
13. S. Durrleman, "Affine and non-linear image warping based on landmarks," Lecture Note, University of Utah, http://www.sci.utah.edu/~gerig/CS6640-F2010/Lecture_10_18_Transformations_Durrleman.pdf (2010).

Ondrej Čierny is a graduate student in the Department of Aeronautics and Astronautics at MIT specializing in pointing, acquisition, and tracking systems for nanosatellite laser communications. He received his BS degree in automation and robotics from the Slovak University of Technology (2015) and his MS degree in space science and technology from Luleå University of Technology and University of Würzburg (2017).

Kerri L. Cahoy is an associate professor in the Department of Aeronautics and Astronautics at MIT. She received her BS (2000) degree in electrical engineering from Cornell University and her MS (2002) and PhD (2008) degrees in electrical engineering from Stanford University working with the Radio Science Team on Mars Global Surveyor. She joined the MIT faculty in July 2011 and leads the Space Telecommunications, Astronomy, and Radiation Laboratory (STAR Lab).